Digital Signal Transmission in Magnetic Induction Based Wireless Underground Sensor Networks

Steven Kisseleff, *Student Member, IEEE*, Ian F. Akyildiz, *Fellow, IEEE*, and Wolfgang H. Gerstacker, *Senior Member, IEEE*

***Abstract*—The objective of Wireless Underground Sensor Networks (WUSNs) is to establish an efficient wireless communication in the underground medium. A magnetic induction (MI)-based signal transmission scheme has been proposed to overcome the very harsh propagation conditions in WUSNs. Due to a much lower vulnerability to the environmental changes, the MI technique has been shown to improve the system performance in terms of achievable data rates and coverage compared to the traditional EM wave based transmission. Two different approaches are known from the literature: direct MI transmission and MI waveguides, where many resonant relay circuits are deployed in the latter between the two nodes to be connected. In this work, digital transmission schemes are investigated for MI-WUSNs employing these two approaches. The influence of transmission parameters like symbol duration and modulation scheme are studied and new methods for their optimization are proposed. In this context, significant gains can be achieved compared to the naive straightforward approaches.**

***Index Terms*—Underground communications, magnetic induction based transmission, wireless sensor networks, digital signal processing.**

I. Introduction

THE OBJECTIVE of Wireless Underground Sensor Networks (WUSNs) is to establish an efficient wireless communication in the underground medium. Typical applications for such networks include soil condition monitoring, earthquake prediction, border patrol, etc. [2], [3]. Since the propagation medium is soil, rock, and sand, traditional wireless signal propagation techniques using electromagnetic (EM) waves can only be applied for very small transmission ranges due to a high path loss and vulnerability to changes of soil properties, such as moisture [4], [5].

Manuscript received November 21, 2014; revised March 13, 2015; accepted April 18, 2015. Date of publication April 23, 2015; date of current version June 12, 2015. This paper has been presented in part in the Proceedings of the IEEE ICC 2014 [1]. This work has been supported by the German Research Foundation (Deutsche Forschungsgemeinschaft, DFG) under Grant No. GE 861/4-1 and in part by the USA National Science Foundation under Grant No. 1320758. The associate editor coordinating the review of this paper and approving it for publication was S. Gezici.

S. Kisseleff and W. H. Gerstacker are with the Institute for Digital Communications, Friedrich-Alexander-University Erlangen-Nürnberg (FAU), 91054 Erlangen, Germany (e-mail: kisseleff@LNT.de; gersta@LNT.de).

I. F. Akyildiz is with the Broadband Wireless Networking Laboratory, School of Electrical and Computer Engineering, Georgia Institute of Technology, Atlanta, GA 30332 USA (e-mail: ian@ece.gatech.edu).

Color versions of one or more of the figures in this paper are available online at http://ieeexplore.ieee.org.

Digital Object Identifier 10.1109/TCOMM.2015.2425891

Magnetic induction (MI) based communication has been already investigated in various works, mostly in the context of near-field communication (NFC) and wireless power transfer [6]–[13]. These studies provide some insight into design aspects of point-to-point MI based signal transmissions.

MI based WUSNs were first introduced in [3] and make use of magnetic antennas implemented as coils, which can be combined in waveguide structures with several passive relay devices between two transceiver nodes according to [14]–[17]. Similar to traditional wireless relaying concepts, the MI transmission benefits from a lower equivalent path loss. Consequently, the transmission range can be greatly increased compared to the EM waves based approach for WUSNs [3].

In previous work, some efforts have been made to characterize the channel conditions of MI-based transmission. Magneto-inductive waveguides with metamaterials are considered in [16], where the signal is described as an MI wave traveling through the channel. Based on this a corresponding noise model is proposed in [18]. Some channel models for MI-WUSNs with frequency-selective path loss are introduced in [9], [14], and [19]. More realistic channel and noise models for a point-to-point transmission are derived in [20]. These models incorporate the losses due to the transmission medium and the power reflections between the coils. Furthermore, it is shown that a transmission through a conductive medium like soil can only be established using a carefully optimized set of system parameters. Based on this work [20], different sets of optimal parameters are proposed in [21] for MI waveguides with a high relay density in WUSNs. In [22], a set of system parameters is determined for direct MI transmission (without relays) for maximizing the throughput of WUSNs. The previous works mostly consider the channel capacity as a performance measure. However, the real methods of digital transmission for WUSNs have not been published yet.

In this work, to establish a fundamental insight into the transceiver design for MI-WUSNs, we employ the system modeling strategies from [20], which provide sufficient information about the channel characteristics. According to [20], due to the losses in the medium, MI waveguides with low relay densities are not applicable, because even for the optimal system parameters the resulting channel capacity of such links is below that of the direct MI transmission with no relays deployed. However, if the relay density is large, the coupling between coils is strong enough to cope with losses, resulting in an increased channel capacity. Therefore, we investigate two cases:

1) direct MI transmission with no relays used and
2) MI waveguides with a high relay density of $\approx \frac{1\ \text{Relay}}{3\ \text{m}}$.

Furthermore, we extend the existing channel and noise models by taking into account the inhomogeneity of the transmission medium, which heavily affects the MI waveguides based transmissions. This issue has been frequently overlooked in the previous studies by assuming a medium with constant properties over space and time. However, a practical system needs to be able to cope with these imperfections.

In summary, we address the issues mentioned in the following.

- We derive more general channel and noise models, which incorporate the influence of the medium inhomogeneity that can become crucial for the signal transmission, especially in case of MI waveguides.
- For the two cases described above (direct MI transmission and MI waveguides), we determine the most efficient transmission bandwidth, which implies also the symbol duration.
- We analyze the performance of the MI based transmission by means of the signal-to-noise ratio per transmitted data symbol in order to determine the optimal modulation scheme, which is still an open issue for underground communication [3].
- For each type of transmission channel, we show an approach to minimize the data rate losses due to modulation schemes with finite alphabet size.
- Furthermore, we investigate how a modulation scheme should be chosen according to the performance requirements and in case of environmental changes. To this end, we consider block based transmissions with the possibility of a retransmission in case of a block error.
- We extend the proposed approaches by taking into account error propagation in the capacity achieving decision-feedback equalization scheme and the need of utilizing training sequences for a stable signal detection and channel estimation. This provides a solid background for future transceiver design and system adaptation.

To enable a coded transmission, a proper coding scheme has to be chosen. For WUSNs, the encoder and decoder design will differ from the designs for traditional cellular systems, since the complexity of both transmitter and receiver should be low from the perspective of the energy consumption. Hence, the choice of the code can be seen as an optimization problem with practical constraints with respect to, e.g., target error rate, code rate, and complexity. This issue requires further exhaustive investigations, which are beyond the scope of this work. Thus, we focus on modulation schemes and filter design for uncoded transmission, which should provide a good basis for the future development of coded transmission in WUSNs.

This paper is organized as follows. In Section II, the system model is presented and the signal processing components within the MI transceivers are specified. In Section III, modulation and equalization for MI based transmission are addressed and the key solutions are given. Section IV provides simulation results and Section V concludes the paper.

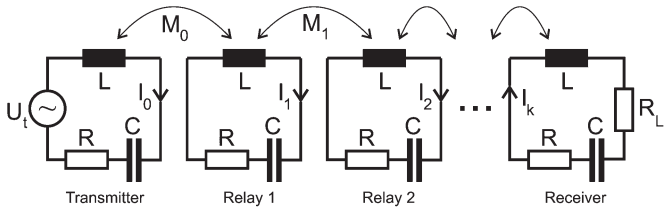

Fig. 1. MI waveguide with unequal coupling between coils.

II. System Modeling

Similar to [14], we assume that the waveguide structure contains one transmitter circuit with a voltage source U_t, one receiver circuit with a load resistor R_L, and $(k-1)$ passive relays, which are placed equidistantly between the transceivers, as shown in Fig. 1. If no relays are deployed, the transmitter induces the voltage directly into the receiver circuit. Each circuit includes a magnetic antenna (which is realized by a multilayer air core coil), a capacitor C, and a resistor R (which models the copper resistance of the coil and depends on the wire radius). The inductivity of a multilayer coil is given by [23], [24]

$$L = \frac{21\mu N^2 a}{4\pi}\left(\frac{a}{l+h}\right)^{0.5}, \tag{1}$$

where N denotes the number of windings, a is the radius of the coil, $l = 0.5\,a$ is the length of the coil [23], h is the height of the windings over the coil surface, and μ denotes the permeability of the soil. The copper resistance of the coil is given by [23]

$$R = \rho \cdot \frac{l_w}{A_w} = \rho \cdot \frac{2aN}{r_w^2}, \tag{2}$$

where $\rho \approx 1.678 \cdot 10^{-2}\ \Omega \cdot \text{mm}^2/\text{m}$ is the copper resistivity, l_w denotes the total wire length, A_w is the cross-section area of the wire, and r_w is the radius of the wire. The capacitance of the capacitor is chosen to make each circuit resonant at frequency f_0 [14], i.e., $C = \frac{1}{(2\pi f_0)^2 L}$. We do not consider parasitic effects, such as skin effect in windings, proximity effect, and parasitic capacities, which may occur in circuit elements at very high frequencies. Instead, it is assumed that in the frequency band used for transmission the influence of these effects is negligible. The induced voltage is related to the coupling between the coils, which is determined by the mutual inductance [25]

$$M_n = \mu\pi N^2 \frac{a^4}{4r_n^3} \cdot J_n \cdot G_n, \tag{3}$$

where r_n denotes the distance between coil n and $n+1$. J_n represents the polarization factor, which depends on the alignment of the coils [22]. G_n is an additional loss factor due to eddy currents as pointed out in [20]. This effect yields an exponential decrease of the field strength with the transmission distance similar to the skin effect in copper wires [26]. In the following, the total transmission distance is denoted by d.

Because all involved signal mappings are linear for MI based transmission, a linear channel model results.

A. Channel and Noise

Here, we derive more precise and valid channel and noise models than the currently existing ones, e.g., [20], in order to take into account the effect of possible medium inhomogeneity. Basically, the usual assumption of a fully homogeneous medium with constant properties seems to be not always valid due to the inhomogeneous nature of soil, irrigation, plants, etc. In particular, non-uniform distribution of the water content in soil is very intuitive and is also the reason for utilizing WUSNs in agriculture, see Section I. Obviously, this non-uniform distribution of water affects the conductivity of the medium. Since the path loss of MI based transmissions heavily depends on the conductivity [20], the variation of medium properties (water content) can dramatically change the frequency-selectivity of the transmission channel and the overall system performance. Hence, a precise modeling of these effects is needed in order to design a robust communication system. In the following, we investigate the influence of a variation of the medium properties on the direct MI transmission and on the MI waveguides based signal propagation.

1) Direct MI Transmission: For the direct MI transmission, the inhomogeneity only affects the conductivity based loss factor $G_n = G_0$ in (3). Hence, the channel transfer function can be given according to [1]

$$H(f) = \frac{I_k R_L}{U_t} = \frac{x_L}{x^2 - 1 + x \cdot x_L}, \tag{4}$$

with $Z = R + j2\pi fL + \frac{1}{j2\pi fC}$, $x = \frac{Z}{j2\pi fM_0}$, $x_L = \frac{R_L}{j2\pi fM_0}$, and with the current flow in the receiver circuit I_k. Furthermore, (4) already incorporates the well known effect of frequency splitting in MI based communication channels [27]. This effect becomes significant in the near field of the induction coils, in case of strong coupling. Then, the magnitude of the denominator in (4) has two minima at two different frequencies around the resonance frequency. In case of weak coupling, $H(f)$ in (4) can be approximated by $H(f) \approx \frac{j2\pi fM_0 \cdot R_L}{Z^2 + Z \cdot R_L}$ with only one maximum at the resonance frequency. For direct MI based trans missions, the coupling between coils is weak due to large distances between coils. Hence, frequency splitting does not occur.

Assuming that the strength of the magnetic field decreases due to the losses in the medium according to $\mathrm{e}^{-\frac{\Delta r_i}{\delta_i}}$ for propagation through the soil with the skin depth δ_i over a distance Δr_i with $\sum_i \Delta r_i = d$, the total decrease of the field strength can be described by

$$G_0 = \prod_i \mathrm{e}^{-\frac{\Delta r_i}{\delta_i}} = \mathrm{e}^{-\sum_i \frac{\Delta r_i}{\delta_i}}. \tag{5}$$

For a given transmission distance d and $\Delta r_i \to 0$, we obtain

$$G_0 = \mathrm{e}^{-\int_0^d \frac{1}{\delta(r)} \mathrm{d}r}, \tag{6}$$

where $\delta(r)$ represents the skin depth at the distance r from the transmitter. If we express the resulting loss factor G_0 by means of $G_0 = \mathrm{e}^{-\frac{d}{\delta_{\mathrm{total}}}}$, the equivalent skin depth of the total transmission link can be given by

$$\delta_{\mathrm{total}} = \frac{1}{\frac{1}{d}\int_0^d \frac{1}{\delta(r)} \mathrm{d}r}, \tag{7}$$

which is the harmonic mean value of the local conductivities $\delta(r)$ of the medium between the transmitter and the receiver. This result is quite intuitive, since the harmonic mean value is more vulnerable to the small values of the local skin depth, which can be seen as bottlenecks for the propagation of the magnetic field. G_0 as defined in (6) is then used in (3) instead of the loss factor of a homogeneous medium.

The receive noise power density spectrum for direct MI based transmission can be obtained as a special case of the noise power density spectrum for MI waveguides, which will be derived in 2).

2) MI Waveguides: For the MI waveguides, one additional reason for the changes in propagation characteristics compared to the propagation assumed at the system design stage is due to the deployment imperfections. Here, small misplacements of the coils and their misorientation may lead to additional signal reflections, which have not been considered in any previous works on MI waveguides based systems.

We start with the assumption of constant circuit elements, which are the result of mass production, thus its tolerances are negligibly small. Therefore, the only difference compared to the assumptions of the channel models proposed in [20] are unequal magnetic couplings between any two adjacent coils of the waveguide. We denote the mutual inductance between coil n and $n+1$ as M_n, cf. (3). Similarly to [20], we start with the basic voltage equation in the receiver

$$(Z + R_L) I_k - j2\pi f M_{k-1} I_{k-1} = 0, \tag{8}$$

where I_n stands for the current flow in coil n, such that I_k is the current flow in the receiver circuit, as shown in Fig. 1. Furthermore, we define $x_n = \frac{Z}{j2\pi fM_n}$ and $x_{L,n} = \frac{R_L}{j2\pi fM_n}$. In addition, we utilize the voltage equation for circuit n

$$Z \cdot I_n - j2\pi f M_{n-1} I_{n-1} - j2\pi f M_n I_{n+1} = 0. \tag{9}$$

Using a similar recursive current calculation like in [20], we arrive at

$$I_n = I_{n-1} \cdot \frac{S(k-n)}{S(k-n+1)}, \tag{10}$$

where the function $S(m)$ is defined in the following way:

$$S(m) = x_{k-m} S(m-1) - \frac{M_{k-m+1}}{M_{k-m}} S(m-2),$$
$$\forall 0 \le m \le k-1,\ S(0) = 1,\ S(1) = x_{k-1} + x_{L,k-1}. \tag{11}$$

with $M_{-1} = M_0$. Obviously, for $M_i = M_0\ \forall i$, the resulting function $S(m)$ is identical with the corresponding function proposed in [20]. Similarly to the reverse calculation provided in [20], the current flow in the transmitter and receiver circuits,

I_0 and I_k, respectively, can be calculated as

$$I_0 = \frac{U_t}{j2\pi f M_0} \cdot \frac{S(k)}{S(k+1)}, \tag{12}$$

$$I_k = \frac{U_t}{j2\pi f M_0} \cdot \frac{1}{S(k+1)}. \tag{13}$$

Hence, the channel transfer function $H(f)$ is given by

$$H(f) = \frac{I_k R_L}{U_t} = \frac{x_{L,0}}{S(k+1)}. \tag{14}$$

For simplicity and without loss of generality, we assume in the following that all coils of the waveguide are placed equidistantly between transmitter and receiver. In the special case of weak couplings between coils, which leads to $x_n \gg 1\ \forall n$, the resulting transfer function can be approximated by

$$H(f) \approx \frac{x_{L,0}}{x_0 \cdot (x_{k-1} + x_{L,k-1}) \cdot \prod_{n=0}^{k-2} x_n} \propto \prod_{n=0}^{k-1} M_n. \tag{15}$$

Hence, assuming that all parameters except for the environmental ones remain constant, the overall skin depth can be expressed by

$$\delta_{\text{total}} = \frac{1}{\frac{1}{k}\sum_{n=0}^{k-1} \frac{1}{\delta_n}}, \tag{16}$$

where δ_n denotes the skin depth between coils n and $n+1$. This skin depth can be expressed in terms of (7), where the integration ranges from d_n to d_{n+1}. Here, d_n denotes the distance of the coil n from the transmitter coil. Inserting (7) in δ_n in (16) yields therefore

$$\delta_{\text{total}} = \frac{1}{\frac{1}{k}\sum_{n=0}^{k-1} \frac{k}{d} \int_{d_n}^{d_{n+1}} \frac{1}{\delta(r)} \mathrm{d}r} = \frac{1}{\frac{1}{d}\int_0^d \frac{1}{\delta(r)} \mathrm{d}r}, \tag{17}$$

which is identical with (7). This result is not surprising, since as described in [20] weakly coupled MI waveguides have a very similar behavior as a direct MI transmission. For strongly coupled waveguides, the approximation (15) is not valid, such that a total skin depth δ_{total} does not exist and no conclusion about the vulnerability of the waveguide to the inhomogeneity of the medium can be made. For all following results, we assume that the medium is homogeneous between any pair of neighboring coils but may vary from pair to pair.

The noise power density spectrum is obtained via summation of the contributions from the noise sources within the waveguide. Due to a strong coupling between the coils for the optimal choice of the system parameters, noise contributions of all sources need to be taken into account. In this work, we focus on the thermal noise, which occurs in the copper wire of the coils and at the load impedance in the receiver circuit. The noise signals are modeled as voltage sources $U_{N,n}\ \forall n$ for the respective coils. Therefore, we need to modify the voltage equations given above as follows:

$$(x_{k-1} + x_{L,k-1}) I_k - I_{k-1} + \frac{U_{N,k}}{j2\pi f M_{k-1}} = 0, \tag{18}$$

$$x_{n-1} I_n - I_{n-1} - \frac{M_n I_{n+1}}{M_{n-1}} + \frac{U_{N,n}}{j2\pi f M_{n-1}} = 0, \quad \forall\ 1 \le n \le k-1. \tag{19}$$

After several substitution and reordering steps, we obtain

$$I_1 = I_0 \cdot \frac{S(k-1)}{S(k)} - \sum_{m=0}^{k-1} \frac{U_{N,k-m}}{j2\pi f M_0} \cdot \frac{S(m)}{S(k)}. \tag{20}$$

By using the modified voltage equation of the transmitter circuit and exploiting the superposition principle, such that the source of the useful signal is replaced by a short-cut, the noise current flow in the transmitter can be obtained via

$$I_0 = \sum_{m=0}^{k} \frac{U_{N,k-m}}{j2\pi f M_0} \cdot \frac{S(m)}{S(k+1)}. \tag{21}$$

Correspondingly, the noise current flow in the receiver is given by

$$I_k = \sum_{l=0}^{k} \frac{\sum_{m=0}^{k-l} U_{N,k-m} \cdot S(m)}{j2\pi f M_{l-1} \cdot S(k-l) \cdot S(k-l+1)}. \tag{22}$$

The receive noise power density spectrum at the load impedance of the receiver is obtained via summation of the noise contributions from all coils. The power spectral density of the assumed Johnson-noise [28] produced by resistor R is given by $4K_B T_K R$ at any frequency f, where $K_B \approx 1.38 \cdot 10^{-23}$ J/K is the Boltzmann constant, T_K is the temperature in Kelvin ($T_K = 290$ K in this work), and $\mathrm{E}\{\cdot\}$ denotes the expectation operator. In addition to the noise signals from the wire resistors R, there is a noise contribution from the load resistor R_L in the receiver circuit. Hence,

$$\mathrm{E}\{P_{\text{noise}}(f)\} = \mathrm{E}\{P_{N,R}(f)\} + \mathrm{E}\{P_{N,R_L}(f)\}, \tag{23}$$

$$\mathrm{E}\{P_{N,R}(f)\} = \frac{4K_B T_K R R_L}{2} \times \sum_{m=0}^{k} \left| \sum_{l=0}^{k-m} \frac{|S(m)|}{j2\pi f M_{l-1} S(k-l) S(k-l+1)} \right|^2, \tag{24}$$

$$\mathrm{E}\{P_{N,R_L}(f)\} = \frac{4K_B T_K R_L^2}{2} \times \left| \sum_{l=0}^{k} \frac{1}{j2\pi f M_{l-1} S(k-l) S(k-l+1)} \right|^2 \tag{25}$$

results for the receive noise power density spectrum, cf. [20]. For direct MI based transmissions, the receive noise power density spectrum can be calculated as a special case of (23) with $k = 1$.

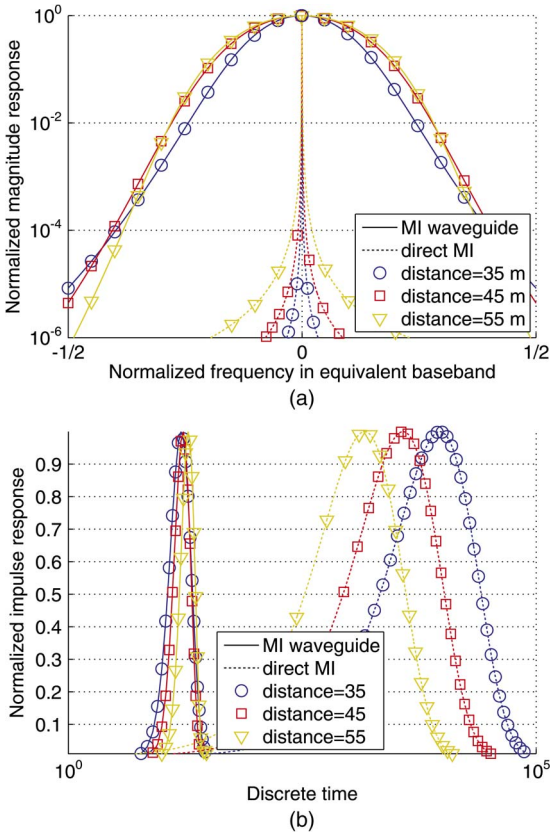

Fig. 2. Examples for MI-based transmission channels: (a) magnitude of frequency response; (b) impulse response.

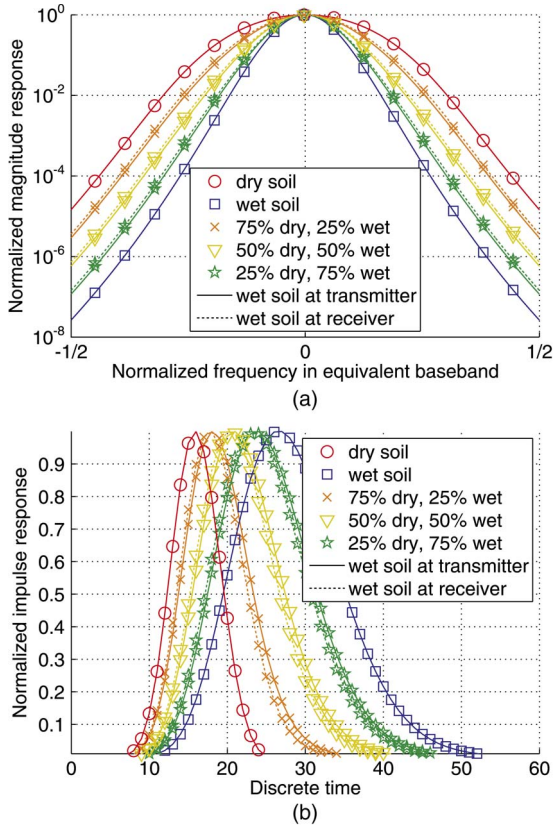

Fig. 3. Examples of the influence of soil moisture on MI waveguides: (a) magnitude of frequency response; (b) impulse response.

B. Examples of the Magnitude and Impulse Responses

Some examples for the transfer functions for different constellations deployed in a homogeneous environment are depicted in Fig. 2(a).[1] It seems not possible to give a closed-form solution for the corresponding impulse responses in time domain shown in Fig. 2(b) which have been calculated by numerical inverse Fourier transform. We observe a much more frequency-selective magnitude response for the direct MI transmission compared to the MI waveguides. In time domain, the impulse responses of the MI waveguides are relatively short (10-15 taps). In contrast, for the direct MI transmission, the impulse response is very long (up to 10^5 taps). As known from the literature [29], the frequency-selectivity of the direct MI transmission does not change much in case of environmental changes, such that only the varying attenuation needs to be compensated. On the contrary, for the MI waveguides, these changes may influence the power reflections between relay coils, such that the resulting frequency-selectivity of the transmission channel changes. To visualize this effect, we show the magnitude and impulse responses for an MI waveguide for 50 m transmission distance, which is optimized (using the methods, which will be discussed later) for the operation in dry soil, see Fig. 3(a) and (b). Here, we consider a completely dry soil, wet soil, and cases of partially wet soil, where the water shed can occupy 25%, 50%, or 75% of the waveguide length. Throughout this work, dry and wet soil are assumed to comply with parameters given in Section IV. These results are calculated using (14) and a corresponding numerical Fourier transform in order to obtain the impulse response. Of course, with weaker couplings between coils the slopes of the magnitude response become more and more steep. Correspondingly, the impulse responses become longer and the peak point shifts more and more in direction of the peak with purely wet soil. Interestingly, not only the amount of water between transmitter and receiver is important, but also the position of the shed. Therefore, we distinguish between the water sheds (wet soil) placed at the transmitter and at the receiver, cf. Fig. 3.

As mentioned earlier, signal reflections inside MI waveguides are inevitable due to the deployment imperfections. In particular, not only the orientation of the coils is a crucial factor, but even small shifts of the relays can dramatically change the frequency-selectivity of the channel and deteriorate the performance. To visualize this effect, an MI waveguide with a total length of 50 m is optimized under the assumption of an equidistant relay deployment. Then, each relay is randomly shifted towards the transmitter or the receiver. This random shift is governed by a normal distribution with a standard deviation of 10 cm or 20 cm. In Fig. 4, some examples of the resulting magnitude frequency responses and impulse responses are depicted, which are normalized by the maximum of the respective response for equidistant (optimal) deployment. Obviously, the

[1]Here, the frequency in equivalent baseband has been normalized by $\frac{1}{T}$, where T is the symbol interval, which has been independently optimized for each MI based transmission channel with regard to the achievable data rate.

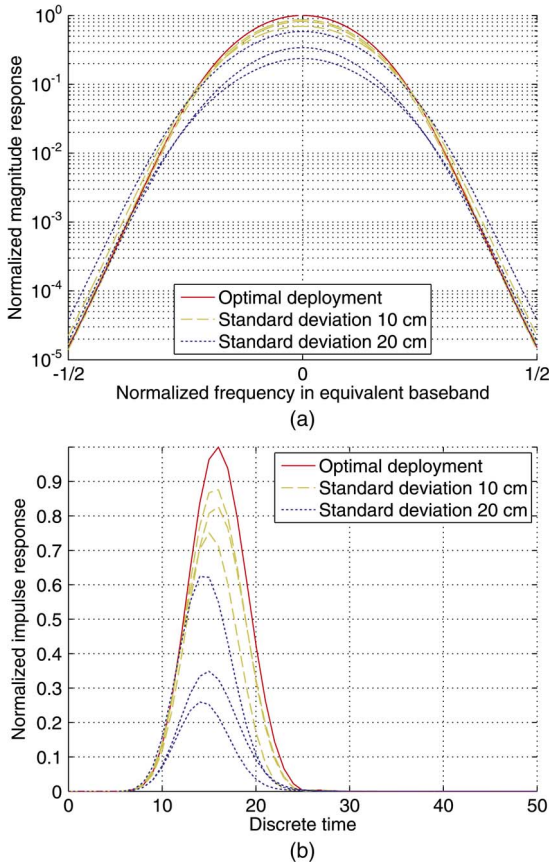

Fig. 4. Examples of the influence of random relay shifts on MI waveguides: (a) magnitude of frequency response; (b) impulse response.

maximum distance between the relays increases with increasing standard deviation. The corresponding path loss increases as well and becomes a dominant factor for the performance of MI waveguides. Hence, even with a small standard deviation of 20 cm, additional path loss of up to 12 dB can be observed.

For the system design and optimization, we consider digital transmissions in homogeneous medium in the following, that can be assumed for environments with nearly constant propagation characteristics. To guarantee the operability of the system even in case of environmental (possibly inhomogeneous) changes, a channel estimation can be applied in order to adjust the transmit power and/or filter coefficients of the digital filters. This can be done either using the traditional receiver-side channel estimation approaches or the transmitter-side channel estimation for MI based communications of [29]. Furthermore, we address the problem of error propagation in MI based signal transmissions, which makes the transmissions of training sequences as part of each data block absolutely necessary. These training sequences can be then used, e.g., for the aforementioned channel estimation.

C. Optimal System Parameters

As it was shown in [20], the general optimization problem of maximizing the channel capacity for MI based transmission (both for direct MI transmission and MI waveguides) is non-convex. However, suboptimal solutions for direct MI transmission and MI waveguides based transmission were proposed in [22] and [21], respectively. We borrow the following equations for the optimum frequency f_0 from these works, assuming an equidistant deployment in a homogeneous medium (usual assumption for the system design).

1) Direct MI Transmission:

$$f_0 = \left(\frac{2}{d\sqrt{\pi\sigma\mu}} \right)^2, \tag{26}$$

where σ denotes the assumed conductivity of the soil. The number of coil windings N is set to the maximum value restricted only by the coil size.

2) MI Waveguides:

$$f_0 = \frac{1}{2\pi\sqrt{L(N)C_0}}, \tag{27}$$

where C_0 stands for the minimum allowed capacitance of the capacitor as pointed out in [20] and $L(N)$ indicates that the inductivity L depends on N. Here, a full search with respect to the discrete variable N can be applied to maximize the channel capacity.

D. Filter Design

In a practical system, the channel capacity from [20], [25], or the network throughput from [21], [22], are not the proper measures for the achievable data rate. Specifically, the transmit pulse was usually assumed to comply with the water filling rule which maximizes the channel capacity [30]. Such pulses are not applicable in practice in general. Instead, a smooth band-limited waveform is used for pulse shaping. Given the transmit filter $A \cdot H_t(f)$ with the amplification coefficient A, the total consumed transmit power P_t results directly from (12),

$$P_t = \frac{1}{2} \int_B \frac{|A \cdot H_t(f)|^2}{|j2\pi f M_0|} \frac{|S(k)|}{|S(k+1)|} \, \mathrm{d}f, \tag{28}$$

where B is the bandwidth of the transmitted waveform. Factor A can be determined to fulfill a given transmit power constraint. The resulting achievable data rate can be calculated using Shannon's capacity equation[2]

$$R_a = \int_B \log_2 \left(1 + \frac{|A \cdot H_t(f) \cdot H(f)|^2}{\mathrm{E}\{P_{\mathrm{noise}}(f)\} \cdot (2R_L)} \right) \mathrm{d}f, \tag{29}$$

where $H(f)$ and $\mathrm{E}\{P_{\mathrm{noise}}(f)\}$ are defined in (14) and (23), respectively.[3]

A realistic approach for the filter design utilizes a square-root Nyquist transmit filter like a root-raised cosine (RRC) filter, which however does not maximize the achievable data rate. Though, the bandwidth of the filter is optimized in order to

[2]For a correct calculation, $|A \cdot H_t(f) \cdot H(f)|^2$ needs to be divided by $(2R_L)$, such that a received signal power density at the frequency f results.

[3]A part of the transmit power density spectrum, $\frac{|S(k)|}{|j2\pi f M_0| \cdot |S(k+1)|}$, is already included in $|H(f)|^2$, because the transmitter circuit is viewed as a part of the transmission channel in MI-based links.

maximize the resulting data rate. For receive filtering we employ the whitened matched filter (WMF) [31]. Here, the overall channel becomes minimum-phase, and the noise after sampling is white. Since the total transmission channel is frequency-selective, an equalization scheme is needed for the signal detection. To avoid further losses in data rate, for our performance investigations we use a decision-feedback equalization (DFE) scheme, which minimizes the mean-squared error (MSE) of the output signal (MMSE-DFE). For coded transmission, the use of MMSE-DFE equalization should be avoided due to error propagation. Instead, Tomlinson-Harashima Precoding (THP) at the transmitter side is recommended [32].

III. Modulation and Coding

To provide specific design rules, we give recommendations for selection of a modulation scheme and symbol rate. For a given target symbol error rate (SER_t), e.g., $\mathrm{SER}_t = 10^{-3}$, and a signal-to-noise ratio (SNR) at the output of the equalizer SNR_{eq}, the constellation size M of the modulation scheme for a maximum data rate under the given performance constraint can be determined using the equations from [33], e.g., for M_{QAM}-ary QAM modulation type

$$\mathrm{SER}_t \geq 4 \cdot Q\left(\sqrt{\frac{3 \cdot \mathrm{SNR}_{eq} K}{M_{QAM}-1}}\right), \tag{30}$$

where M_{QAM} denotes the constellation size, $Q(\cdot)$ is the complementary Gaussian error integral, and K stands for the coding gain of the employed channel code [34]. This leads to

$$\log_2 M_{QAM} = \left\lfloor \log_2\left(1 + \frac{3 \cdot \mathrm{SNR}_{eq} K}{c}\right)\right\rfloor, \tag{31}$$

with a constant $c = \left(Q^{-1}\left(\frac{\mathrm{SER}_t}{4}\right)\right)^2$, where $Q^{-1}(\cdot)$ represents the inverse of the function $Q(\cdot)$. The $\lfloor\cdot\rfloor$ operator is applied, because we restrict our constellation sizes to powers of two. The overall data rate equals $R_d = \frac{R_c \log_2 M_{QAM}}{T}$, where R_c is the code rate and T denotes the symbol interval. If realistic codes with finite lengths are applied in a practical system, the corresponding coding gain K at the target SER should be used for the calculation. The modulation scheme and the code itself should be chosen to maximize the overall data rate. In addition, the complexity of encoding and decoding is very crucial for the low-power sensor nodes and needs to be taken into account, as argued before. This issue is however beyond the scope of this work. Therefore, in the following, uncoded transmission with $K = 1$ and $R_c = 1$ is considered.

A. Problems of MI Based Transmissions

As mentioned before, we consider the direct MI transmission scheme and the MI waveguide based scheme with a high relay density in this work. There is a significant difference in the nature of the two approaches. For the direct MI transmission, the data rate is maximized, if the carrier frequency is low due to the frequency dependent eddy currents effect. For MI waveguides, the optimal carrier frequency is much higher, because the coupling between adjacent coils is much stronger due to short distances between relay coils. In addition, the slopes of the channel transfer function are much steeper for MI waveguides than for the direct MI transmission. This is due to the fact, that every additional relay attenuates the slopes of the channel frequency response further. Therefore, the optimal transmission bandwidth for the direct MI transmission is larger than that for the MI waveguides. However, the region of low path loss of the direct MI channel is very narrow, such that the channel impulse response is very long (up to several 10 000 taps), see Fig. 2. Such channels cannot be equalized in a practical system. In particular, if MMSE-DFE is applied after the WMF, the feedback filter of DFE needs to have roughly the length of the channel for a good performance. However, a feedback filter with 10 000 taps is not realistic and also would produce severe error propagation.

As mentioned earlier, the optimal transmit bandwidth for the MI waveguide channels is very low, even if a high data rate is achievable. From this we deduce a very high SNR, which allows for a choice of a higher order modulation scheme. In addition, due to a transmission in a narrow band, the fluctuations within the band are very limited (see Fig. 2(a)), such that the corresponding impulse response is short (below 10 taps). However, for many cases in waveguide transmission the SNR at the output of the equalizer is high enough to enable a modulation with 14–18 bit/symbol, which cannot be implemented. In these cases, even if a modulation order of 10 bit/symbol (which corresponds to 1024-QAM modulation[4]) is selected, the achievable data rate decreases by $1 - \frac{10\mathrm{bit}}{18\mathrm{bit}} \approx 45\%$. The losses compared to the channel capacity are, of course, even higher. We refer to this method as clipping.

B. Proposed Solutions

1) Direct MI Transmission: For the direct MI channels, the problems arising from long impulse responses can be resolved by reducing the bandwidth. Hence, the width of the low path loss band increases relatively to the symbol rate, thus reducing the number of channel taps. We choose the bandwidth (and therefore the symbol rate), for which the number of channel taps observed at the input of the equalizer is about 100. This strategy enables a practical realization of the equalizer filters and therefore of a real transmission system. We refer to this method as our default scheme. However, due to a much smaller bandwidth losses of up to 98% of the achievable data rate are inevitable. Unfortunately, it is impossible to reduce these losses using conventional single-carrier transmission while maintaining a discrete-time channel impulse response with limited support.

In a different approach, the total band is split in parts, which are processed independently, similar to the traditional frequency-division multiplexing (FDM) approach with multiple sub-bands. Frequency-division is utilized in this context due to a very steep transition between the low path loss band and the side bands. Here, three transmission bands are chosen, in order

[4]Higher order modulation schemes beyond 1024-QAM are not considered in this work due to their high complexity, such that they are not applicable in the low-power sensor node transceivers.

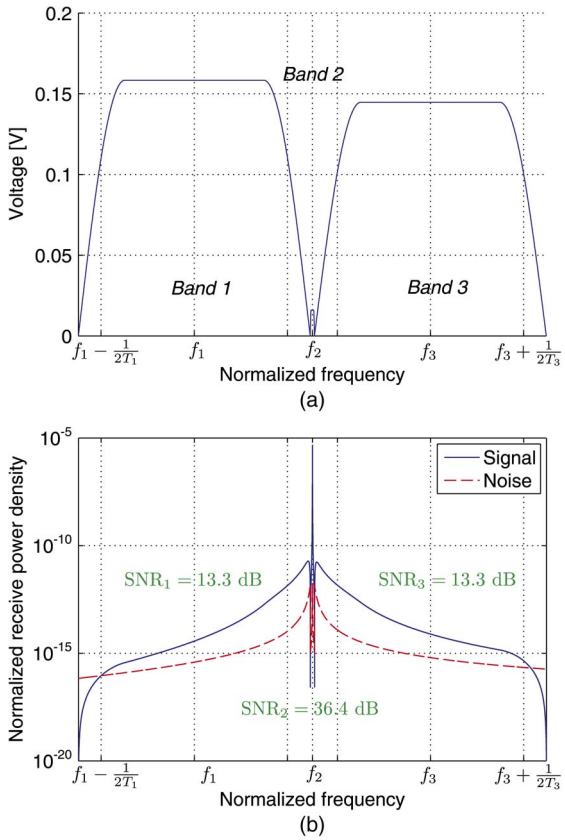

Fig. 5. Spectrum division for transmission distance $d = 35$ m. (a) Transmit spectra in three frequency bands with center frequencies f_1, f_2, and f_3 using power allocation; the corresponding symbol intervals are T_1, T_2, and T_3; (b) Received power density spectra (normalized to 1 W received power per sub-band) and SNR at the equalizer output.

to keep the transceiver design as simple as possible, see Fig. 5. These bands are processed independently at the receiver using WMFs, which contain RRC filters as parts of the analogue matched filters. Hence, due to the frequency-selectivity of the RRC filters, there is no power dissipation to the neighboring bands and no intercarrier interference (ICI). The width of the inner band (band 2) is determined according to the specified maximum length of the channel impulse response as described earlier. The other two bands (band 1 and band 3) occupy the remaining left and right parts of the spectrum, respectively. Due to a larger path loss at the edges of the spectrum than at the resonance frequency, the SNRs for band 1 and band 3 may be very limited if equal power is allocated to all bands, such that no transmission is feasible in the side bands. On the contrary, due to a very low path loss at the resonance frequency, the SNR for band 2 is very high, which enables a modulation with 10–12 bit/symbol. To provide a modulation of at least 1 bit/symbol (BPSK), the bands 2 and 3 need to be allocated more transmit power under the constraint $P_t = P_1 + P_2 + P_3$, where P_i, $i = 1, 2, 3$ is the transmit power in transmission band i. Due to the small number of bands, the problem of finding the optimal power allocation with respect to the achievable data rate can be solved by exploiting the symmetry of the bands. Then a full search in one variable, which corresponds to the power allocated to the inner band, can be performed. With increasing number of sub-bands, the performance tends to approach the channel capacity because of the power allocation which approaches that of the water filling rule. Similarly, an orthogonal FDM (OFDM) scheme can be applied, which is beneficial for a large number of subcarriers. However, in order to decouple the OFDM blocks and to enable cyclic convolution in OFDM, a guard interval has to be chosen at least as long as the channel impulse response, which has a length of over 10 000 taps. Even if an appropriate channel shortening filter (with at most 100 taps) is applied, the resulting impulse response is still very long, yielding a reduction of the data rate. Therefore, the practicality and efficiency of OFDM for the direct MI transmission in WUSNs still remains to be verified.

2) MI Waveguides: As mentioned earlier, the bandwidth of the MI waveguides based channels is very limited. To reduce the loss of the clipping strategy, the bandwidth is chosen larger than the optimal bandwidth, which maximizes the data rate with unlimited constellation size. Hence, the SNR decreases and SER becomes worse, because less power is allocated to the frequencies with low path loss. This disadvantage is partially compensated for by the increased bandwidth/symbol rate. In fact, we convert the benefit of a large SNR into the benefit of a large bandwidth. We increase the bandwidth until the SER fulfills the target SER constraint with equality for the chosen modulation scheme (here: 1024-QAM). A further increase in bandwidth (along with a reduction of M_{QAM}) may lead to longer impulse responses with more than 100 taps and is therefore not considered in this work.

C. Error Propagation

As known from the literature, the error propagation in decision-feedback equalizers can dramatically increase SER and reduce the system performance, even if a long training sequence is used as a preamble of the transmitted data block for feedback filter initialization. This problem aggravates in case of high order modulation schemes, such that after a single error all the remaining symbols of the block are erroneous as well. Especially for the mid sub-band of the direct MI transmission scheme and for the MI waveguides based transmissions this problem leads to a degradation of the symbol error rate of a block, which is either very low (if symbol errors occur not before the end of the block and affect not too many symbols) or very high (up to 0.99). Considering the fact, that the erroneous blocks need to be retransmitted, the number of block retransmissions, which is related to the block error rate (BLER), seems to be a better optimization criterion for our system than SER_t.

Since we utilize uncoded transmissions in this work, we can assume that even a single error cannot be corrected at the receiver. Hence, only the first error in the block is important. This error does not result from the error propagation, but solely from the additive white Gaussian noise. Hence, the total BLER can be given by

$$\text{BLER} = 1 - (1 - \text{SER})^{(N_{BL} - N_{TS})}, \tag{32}$$

where N_{BL} is the block length and N_{TS} stands for the length of the training sequence in the block. Therefore, $(N_{BL} - N_{TS})$

corresponds to the number of data symbols. Due to a constant BLER for all transmitted blocks, the probability of a block error after i retransmissions (i.e., all i transmitted blocks are erroneous) is given by BLER^i. Hence, the expectation value of the number of transmitted and retransmitted symbols of the same block is given by $\sum_{i=0}^{\infty}(N_{BL}\cdot \text{BLER}^i)$. Then, the effective available data rate becomes

$$\begin{aligned} R_{eff} =& R_d \frac{N_{BL}-N_{TS}}{\sum_{i=0}^{\infty}(N_{BL}\cdot \text{BLER}^i)} \\ =& R_d \frac{(N_{BL}-N_{TS})(1-\text{BLER})}{N_{BL}} \\ =& R_d \frac{(N_{BL}-N_{TS})(1-\text{SER})^{(N_{BL}-N_{TS})}}{N_{BL}}. \end{aligned} \quad (33)$$

For a given SER, the length of the symbol block can be optimized in order to maximize the effective available data rate. Further calculation yields

$$\begin{aligned} \log(R_{eff}) =& \log(N_{BL}-N_{TS}) - \log(N_{BL}) \\ &+ (N_{BL}-N_{TS})\cdot \log(1-\text{SER}) + \log(R_d). \end{aligned} \quad (34)$$

Then, $\log(R_{eff})$ is maximized by the choice

$$N_{BL} = \frac{N_{TS}}{2}\left(1+\sqrt{1-\frac{4}{N_{TS}\log(1-\text{SER})}}\right), \quad (35)$$

which is rounded to the closest integer number. According to this calculation, the methods proposed in Section III-B need to be modified in the following way.

1) Direct MI Transmission: The power allocation problem for the sub-bands of the proposed transmission scheme can be solved using a full search in one variable P_2, which corresponds to the transmit power in the mid sub-band. Due to the symmetry, the transmit powers in the side bands can be directly calculated based on the total transmit power P_t. In each point of the search, the current SERs are known for a given modulation scheme. Hence, the block length in (35) can be obtained and the metric $R_{eff,i}$ from (33) for each sub-band is calculated for a given power allocation and modulation scheme. In the next step, the optimum modulation schemes are chosen for the given power allocation. Finally, the optimal power allocation is found in this way which maximizes the sum rate $\sum_{i=1}^{3} R_{eff,i}$.

2) MI Waveguides: The proposed increase of the bandwidth yields a large increase in data rate compared to the naive clipping approach. However, the stopping condition of the algorithm needs to be modified, since the condition $\text{SER} = \text{SER}_t$ does not maximize the proposed effective available data rate as described earlier. Therefore, we propose to increase the bandwidth of the transmit spectrum until the maximum of R_{eff} is reached. Since the modulation order M_{QAM} is an available design parameter, it can be determined in each step of the bandwidth extension via full search among all possible modulation schemes.

IV. Numerical Results

In this section, we discuss numerical results for achievable data rates and the modulation order. In our simulations, we assume a total transmit power of $P_t = 10$ mW. We utilize coils with wire radius 0.5 mm and coil radius $a = 0.15$ m. The maximal number of coil windings N is 1000. The conductivity and permittivity of soil are $\sigma = 0.01$ S/m and $\epsilon = 7\epsilon_0$ for dry soil [35] and $\sigma = 0.077$ S/m and $\epsilon = 29\epsilon_0$ for wet soil, respectively, where $\epsilon_0 \approx 8.854\cdot 10^{-12}$ F/m. Since the permeability of soil is close to that of air, we use $\mu = \mu_0$ with the magnetic constant $\mu_0 = 4\pi\cdot 10^{-7}$ H/m. For a reduced path loss, $J_n = 2,\ \forall\ n$ is assumed, which corresponds to the horizontal axes deployment, cf. [20]. The roll-off factor of the used RRC transmit filter is 0.25. Also, we assume $N_{TS} = 150$.

To take into account the influence of inhomogeneous medium properties, the signal equalization has to be done in an adaptive way, e.g., by using a Least-Mean-Square (LMS) based adaptation or a Recursive Least-Squares (RLS) based adaptation. Both schemes iteratively adjust the filter coefficients of the DFE and converge to the optimal equalizer filters for the unknown channel. However, due to the aforementioned error propagation, the convergence of these algorithms cannot be guaranteed. Moreover, after every error the adaptation becomes unstable. Therefore, we propose to apply a channel estimation using a training sequence of length N_{TS} (same N_{TS} as in Section III-C) and then determine the proper equalization filters for the estimated version of the channel impulse response. This approach is rather reliable, because of a very long coherence time in WUSNs due to the rarely changing channel characteristics. Hence, very accurate estimates of the channel coefficients can be acquired and the SER of this transmission is very close to the optimum SER for the given channel, modulation, and coding scheme. In case of an unforeseen additional attenuation of the channel, the modulation and signal transmission policies need to be adjusted accordingly, e.g., by reducing the constellation size M_{QAM} or the total block length N_{BL}. Note that the bandwidth B cannot be modified after the implementation, since it is related to the implemented analog transmit and receive filters, that usually remain unchanged. Hence, we are not allowed to change the bandwidth after the optimization and implementation. In addition, in a larger network with several sensor nodes, especially in networks with MI based transmissions, it can be a challenging task to establish a proper scheduling of signal transmissions, which can be destroyed by arbitrarily adjusting the length of the packet size (equivalent to the block length in this work). Therefore, in a changing environment, we recommend to only adjust the modulation order and leave the block length constant. In the following, we assume a time-invariant environment.

First, we show results on the achievable data rate for direct MI transmission, see Fig. 6. Here, we compare the results of the proposed three-band solution with the theoretical bounds given by channel capacity and single-band approaches. According to Fig. 6, large losses in achievable data rate are observed, if a finite impulse response (FIR) equalizer is used compared to the theoretical upper bound for uncoded transmission using an infinite impulse response (IIR) equalizer. Results for FIR

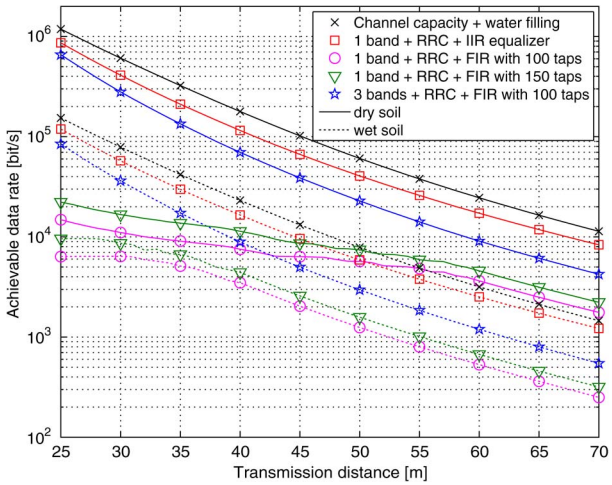

Fig. 6. Achievable data rate for direct MI transmission.

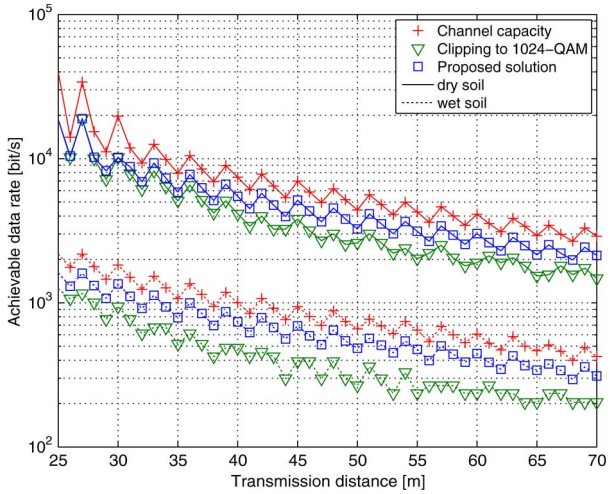

Fig. 7. Achievable data rate for MI waveguides.

filters of length 100 and 150, respectively, are depicted. With increasing length of the equalizer filters, the data rate increases very slowly, such that several thousand filter taps are needed to increase the data rate from ≈22.5 kbit/s for 25 m transmission distance to ≈865 kbit/s. We conclude that the big gap between the data rate of a practical system and the theoretical bound cannot be diminished, if a single-band transmission technique is applied. The proposed solution of utilizing three transmission bands with power allocation performs much better and achieves up to 75% of the theoretical limit of the uncoded single-band transmission. For comparison, we also show the channel capacity for error-free coded transmission. The proposed solution performs between ≈45% and ≈60% worse than the channel capacity, leaving a noticeable gap to be closed via code design.

For MI waveguides, we compare the data rates of the proposed solution of the bandwidth expansion with that of clipping for dry and wet soil, respectively, as shown in Fig. 7. The proposed solution outperforms the clipping approach and performs slightly worse compared to the channel capacity. In addition, we observe that increasing the bandwidth is even more beneficial for deployment in a wet soil environment than in dry soil, where

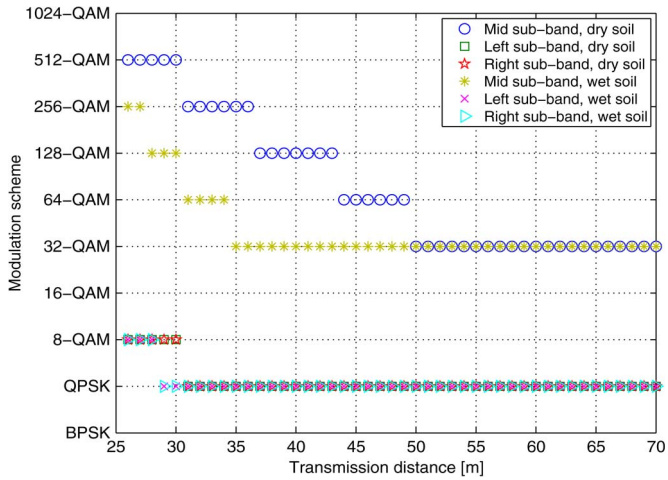

Fig. 8. Proposed modulation schemes for direct MI transmission.

the gain compared to the clipping approach is sometimes very limited. This is due to the reduced bandwidth for transmission in wet soil compared to transmission in dry soil. Hence, the power is more concentrated in a very narrow frequency region, such that a larger SNR results and correspondingly a larger constellation is needed. Similarly, with increasing transmission distance, the gain of the proposed solution compared to the default scheme increases. This fact makes this approach even more suitable for MI-WUSNs based on waveguides, since it has been shown in [20] that MI waveguides only outperform direct MI transmission for distances beyond ≈50 m.

Finally, we investigate the modulation schemes, which should be chosen for an uncoded transmission in order to maximize the data rate under the given assumptions. For the MI waveguides in dry soil, the optimal modulation scheme is mostly the largest allowed constellation (clipping bound), which is 1024-QAM in this work. However, the resulting BLER in (32) is sometimes not enough to keep the number of retransmissions low, such that lower modulation orders with lower BLER are preferred, e.g., 512-QAM. Due to a nonlinear dependency of the path loss function on the transmission distance in MI waveguides based transmissions, these cases do not show any clear trend. In wet soil, the transmission band is even narrower than in dry soil. This leads to a very high SNR, such that BLER is low even in case of high modulation orders. Hence, retransmissions are unlikely and the performance gain of the proposed solution compared to the default scheme is very high in Fig. 7.

For direct MI transmission, we show the proposed modulation schemes for all three sub-bands and deployment in dry and wet soil, respectively, in Fig. 8. The path loss in the inner band is much larger in wet soil medium than in dry soil. Hence, the modulation order in wet soil is lower or equal to the modulation order in dry soil. Furthermore, with transmission distances beyond 50 m the chosen modulation scheme seems to converge towards 32-QAM for the mid sub-band and QPSK for the side bands. The reason for this lies in the additional degrees of freedom, i.e., the optimally chosen block length and power allocation. Thus, it is more advantageous to e.g., reduce the block length, in order to cope with the higher path loss for

longer transmission distances, than to reduce the modulation order, which may lead directly to 20% decrease of data rate for the mid sub-band or even 50% for the side bands. In addition, we observe a large variety of modulation schemes for direct MI transmission, varying between QPSK and 512-QAM. In a larger network with several transmission links, a unification of the transmission and system parameters is needed for a feasible manufacturing. Therefore, an optimal modulation scheme for a set of transmitting devices should be chosen based on the network topology and from the perspective of the network throughput optimization [21], [22]. This investigation is, however, beyond the scope of this work.

V. Conclusion

In this paper, we have considered the design of MI transceivers for uncoded transmission in WUSNs. For the two most relevant cases (direct MI transmission and MI waveguides), we provide more precise channel and noise models, which take into account the possible inhomogeneity of the medium. Then, the maximum achievable data rates, which can be obtained in a point-to-point transmission using realistic transmit, receive, and equalization filters, are investigated. In addition, recommendations for the symbol duration and modulation scheme are given, which maximize the achievable data rate for a specified symbol error rate. For direct MI transmission, the problem of equalizing a very long channel impulse response can be circumvented by utilizing a frequency-division based scheme with three transmission bands. For MI waveguides, a very high modulation order can be avoided using a bandwidth expansion approach. A significant increase in data rate is observed compared to the default transmission schemes. Furthermore, the problem of the error propagation of DFE is addressed and the proposed solutions are modified accordingly, in order to reduce the losses due to possible retransmissions of the erroneous data blocks. Moreover, we emphasize the need of training sequences, which should be employed as part of every transmitted data block, in order to reduce the probability of block errors. In this context, the block length is optimized for a given length of the training sequence, in order to maximize the data rate. Hence, this paper provides a solid background for future transceiver design for MI based WUSNs.

References

[1] S. Kisseleff, I. F. Akyildiz, and W. Gerstacker, "On modulation for magnetic induction based transmission in wireless underground sensor networks," in *Proc. IEEE ICC*, Jun. 2014, pp. 71–76.

[2] I. F. Akyildiz, W. Su, Y. Sankarasubramaniam, and E. Cayirci, "Wireless sensor networks: A survey," *Comput. Netw. J.*, vol. 38, no. 4, pp. 393–422, Mar. 2002.

[3] I. F. Akyildiz and E. P. Stuntebeck, "Wireless underground sensor networks: Research challenges," *Ad Hoc Netw.*, vol. 4, no. 6, pp. 669–686, Nov. 2006.

[4] I. F. Akyildiz, Z. Sun, and M. C. Vuran, "Signal propagation techniques for wireless underground communication networks," *Phys. Commun.*, vol. 2, no. 3, pp. 167–183, Sep. 2009.

[5] L. Li, M. C. Vuran, and I. F. Akyildiz, "Characteristics of underground channel for wireless underground sensor networks," in *Proc. IFIP Mediterranean Ad Hoc Netw. Workshop*, Jun. 2007, pp. 92–99.

[6] R. Bansal, "Near-field magnetic communication," *IEEE Antennas Propag. Mag.*, vol. 46, no. 2, pp. 114–115, Apr. 2004.

[7] A. Karalis, J. D. Joannopoulos, and M. Soljacic, "Efficient wireless non-radiative mid-range energy transfer," *Ann. Phys.*, vol. 323, no. 1, pp. 34–48, Jan. 2008.

[8] J. I. Agbinya and M. Masihpour, "Near field magnetic induction communication link budget: Agbinya-Masihpour model," in *Proc. 5th Int. Conf. IB2Com*, 2010, pp. 1–6.

[9] J. I. Agbinya and M. Masihpour, "Power equations and capacity performance of magnetic induction communication systems," *Wireless Pers. Commun.*, vol. 64, no. 4, pp. 831–845, Jun. 2012.

[10] M. Masihpour, D. Franklin, and M. Abolhasan, "Multihop relay techniques for communication range extension in near-field magnetic induction communication systems," *J. Netw.*, vol. 8, no. 5, pp. 999–1011, May 2013.

[11] K. Lee and D.-H. Cho, "Maximizing the capacity of magnetic induction communication for embedded sensor networks in strongly and loosely coupled regions," *IEEE Trans. Magn.*, vol. 49, no. 9, pp. 5055–5062, Sep. 2013.

[12] S. Cheon, Y.-H. Kim, S.-Y. Kang, M. L. Lee, and T. Zyuing, "Wireless energy transfer system with multiple coils via coupled magnetic resonances," *ETRI J.*, vol. 34, no. 4, pp. 527–535, Aug. 2012.

[13] X. Zhang, S. L. Ho, and W. N. Fu, "Quantitative design and analysis of relay resonators in wireless power transfer system," *IEEE Trans. Magn.*, vol. 48, no. 11, pp. 4026–4029, Nov. 2012.

[14] Z. Sun and I. F. Akyildiz, "Magnetic induction communications for wireless underground sensor networks," *IEEE Trans. Antennas Propag.*, vol. 58, no. 7, pp. 2426–2435, Jul. 2010.

[15] E. Shamonina, V. A. Kalinin, K. H. Ringhofer, and L. Solymar, "Magneto-inductive waveguide," *Electron. Lett.*, vol. 38, no. 8, pp. 371–373, Apr. 2002.

[16] R. R. A. Syms, I. R. Young, and L. Solymar, "Low-loss magneto-inductive waveguides," *J. Phys. D, Appl. Phys.*, vol. 39, no. 18, pp. 3945–3951, Sep. 2006.

[17] E. Shamonina, V. A. Kalinin, K. H. Ringhofer, and L. Solymar, "Magnetoinductive waves in one, two, and three dimensions," *J. Appl. Phys.*, vol. 92, no. 10, pp. 6252–6261, Nov. 2002.

[18] R. R. A. Syms and L. Solymar, "Noise in metamaterials," *J. Appl. Phys.*, vol. 109, no. 12, Jun. 2011, Art. ID. 124909.

[19] H. Jiang and Y. Wang, "Capacity performance of an inductively coupled near field communication system," in *Proc. IEEE Int. Symp. Antenna Propag. Soc.*, Jul. 2008, pp. 1–4.

[20] S. Kisseleff, W. H. Gerstacker, R. Schober, Z. Sun, and I. F. Akyildiz, "Channel capacity of magnetic induction based wireless underground sensor networks under practical constraints," in *Proc. IEEE WCNC*, Apr. 2013, pp. 2603–2608.

[21] S. Kisseleff, W. Gerstacker, Z. Sun, and I. F. Akyildiz, "On the throughput of wireless underground sensor networks using magneto-inductive waveguides," in *Proc. IEEE GLOBECOM*, Dec. 2013, pp. 322–328.

[22] S. Kisseleff, I. F. Akyildiz, and W. Gerstacker, "Interference polarization in magnetic induction based wireless underground sensor networks," in *Proc. IEEE PIMRC—Int. Workshop Wireless SENSA*, Sep. 2013, pp. 71–75.

[23] H.-W. Beckmann *et al.*, *Friedrich Tabellenbuch Elektrotechnik/Elektronik*. Berlin, Germany: Ferd. Dümmlers Verlag, 1998, pp. 553–579.

[24] H. Lindner, H. Brauer, and C. Lehmann, *Taschenbuch der Elektrotechnik und Elektronik*. Leipzig, Germany: Fachbuchverlag Leipzig, ch. 8, 2004.

[25] Z. Sun and I. F. Akyildiz, "On capacity of magnetic induction-based wireless underground sensor networks," in *Proc. IEEE INFOCOM*, Mar. 2012, pp. 370–378.

[26] E. E. Kriezis, T. D. Tsiboukis, S. M. Panas, and J. A. Tegopoulos, "Eddy currents: Theory and applications," *Proc. IEEE*, vol. 80, no. 10, pp. 1559–1589, Oct. 1992.

[27] Y. Zhang, Z. Zhao, and K. Chen, "Frequency splitting analysis of magnetically-coupled resonant wireless power transfer," in *Proc. IEEE ECCE*, Sep. 2013, pp. 2227–2232.

[28] H. T. Friis, "Noise figures of radio receivers," *Proc. IRE*, vol. 32, no. 7, pp. 419–422, Jul. 1944.

[29] S. Kisseleff, I. F. Akyildiz, and W. Gerstacker, "Transmitter-side channel estimation in magnetic induction based communication systems," in *Proc. IEEE BlackSeaCom*, May 2014, pp. 16–21.

[30] D. Tse and P. Viswanath, *Fundamentals of Wireless Communication*. Cambridge, U.K.: Cambridge Univ. Press, 2005.

[31] J. G. Proakis, *Digital Communications*. New York, NY, USA: McGraw-Hill, 2001.

[32] G. D. Forney and G. Ungerboeck, "Modulation and coding for linear Gaussian channels," *IEEE Trans. Inf. Theory*, vol. 44, no. 6, pp. 2384–2415, Oct. 1998.

[33] A. Goldsmith, *Wireless Commun.*. Cambridge, U.K.: Cambridge Univ. Press, 2005.
[34] T. S. Rappaport, *Wireless Communications: Principles and Practice*, 2nd ed. Englewood Cliffs, NJ, USA: Prentice-Hall, 2002.
[35] A. Markham and N. Trigoni, "Magneto-inductive networked rescue system (MINERS) taking sensor networks underground," in *Proc. IPSN*, Apr. 2012, pp. 317–328.

Steven Kisseleff (S'12) received the Dipl.-Ing. degree in information technology with focus on communication engineering from the University of Kaiserslautern, Germany, in 2011. He is currently pursuing the Ph.D. degree in electrical engineering at Friedrich-Alexander-University Erlangen-Nürnberg (FAU).

From 2010 to 2011, he was a Research Assistant with the Fraunhofer Institute of Optronics, System Technologies and Image Exploitation (IOSB). Since 2011, he has been a Research and Teaching Assistant with the Institute for Digital Communication (IDC), Erlangen-Nürnberg (FAU), Germany. His research interests lie in the area of digital communications, wireless sensor networks, and magnetic induction based transmissions.

Mr. Kisseleff was a recipient of Student Travel Grants for IEEE Wireless Communications and Networking Conference (WCNC) 2013 and IEEE International Conference on Communications (ICC) 2014, respectively.

Ian F. Akyildiz (M'86–SM'89–F'96) received the B.S., M.S., and Ph.D. degrees in computer engineering from the University of Erlangen-Nürnberg, Erlangen, Germany, in 1978, 1981, and 1984, respectively. Currently, he is the Ken Byers Chair Professor in Telecommunications with the School of Electrical and Computer Engineering, Georgia Institute of Technology, Atlanta, the Director of the Broadband Wireless Networking Laboratory and Chair of the Telecommunication Group at Georgia Tech.

He is an honorary professor with the School of Electrical Engineering at Universitat Politecnica de Catalunya (UPC) in Barcelona, Catalunya, Spain and founded the N3Cat (NaNoNetworking Center in Catalunya). Since September 2012, he has also been a FiDiPro Professor (Finland Distinguished Professor Program (FiDiPro) supported by the Academy of Finland) at the Department of Communications Engineering, Tampere University of Technology, Finland.

Dr. Akyildiz is the Editor-in-Chief of *Computer Networks* (Elsevier) and the founding Editor-in-Chief of *Ad Hoc Networks* (Elsevier), *Physical Communication* (Elsevier), *Nano Communication Networks* (Elsevier). He is an ACM Fellow (1997). He received numerous awards from IEEE and ACM. His current research interests are in wireless underground sensor networks, nanonetworks, and Long Term Evolution (LTE) advanced networks.

Wolfgang H. Gerstacker (S'93–M'98–SM'11) received the Dipl.-Ing. degree in electrical engineering from the University of Erlangen-Nürnberg, Erlangen, Germany, in 1991, the Dr.-Ing. degree in 1998, and the Habilitation degree in 2004 from the same university. Since 2002, he has been with the Chair of Mobile Communications (now renamed to Institute for Digital Communications) of the University of Erlangen-Nürnberg, currently as a Professor.

His research interests are in the broad area of digital communications and statistical signal processing and include detection, equalization, parameter estimation, MIMO systems and space-time processing, interference management and suppression, resource allocation, relaying, cognitive radio, and sensor networks. He has conducted various projects with partners from industry. He is a recipient of several awards including the Research Award of the German Society for Information Technology (ITG) (2001), the EEEfCOM Innovation Award (2003), the Vodafone Innovation Award (2004), a Best Paper Award of EURASIP Signal Processing (2006), and the "Mobile Satellite & Positioning" Track Paper Award of VTC2011-Spring.

Dr. Gerstacker has been an Editor for the IEEE TRANSACTIONS ON WIRELESS COMMUNICATIONS since 2012. Furthermore, he is an Area Editor for Elsevier *Physical Communication* (PHYCOM), and has served as a Lead Guest Editor of a *PHYCOM* special issue on broadband single-carrier transmission techniques (2013). He has been a Member of the Editorial Board of *EURASIP Journal on Wireless Communications and Networking* from 2004 to 2012. He has served as a Member of the Technical Program Committee of various conferences. He has been a Technical Program Co-Chair of the IEEE International Black Sea Conference on Communications and Networking (BlackSeaCom) 2014 and a Co-Chair of the Cooperative Communications, Distributed MIMO and Relaying Track of VTC2013-Fall.